Natural Hazards
https://doi.org/10.1007/s11069-024-06771-2

ORIGINAL PAPER

A novel approach to stability analysis of random soil-rock mixture slopes using finite element method in ABAQUS

Van-Hoa Cao[1] · **Gyu-Hyun Go**[1]

Received: 7 February 2024 / Accepted: 3 July 2024

Abstract
Minimizing the damage caused by landslide disasters in regions with complex geological conditions requires the development of effective and reliable methods for assessing slope stability. This study aims to generate and analyze the stability of random soil-rock mixture slope models, considering the rock block content, spatial distribution, and convexity-concavity feature of rock blocks in the slope. A Python script was developed to create these random soil-rock mixture models using the ABAQUS finite element software. Additionally, the strength reduction technique was applied to calculate the factor of safety via a USDFLD subroutine implemented in ABAQUS. A series of numerical analyses were conducted to assess the impact of rock block content and the convexity-concavity feature of rock blocks on the stability of soil-rock mixture slopes. Moreover, the impact of the random spatial distribution of rock blocks on the stability of soil-rock mixture slopes was discussed. The results show that rock block content below 20% can affect slope stability both negatively and positively. Notably, significant improvements in the stability of soil-rock mixture slopes are observed only when the rock block content exceeds 30%. Furthermore, the convexity-concavity feature of rock blocks can improve the safety factor of the slopes. This study provides a comprehensive methodology and serves as a valuable reference for estimating the safety factor of soil-rock mixture slopes using the finite element method.

Keywords Soil-rock mixtures · Stability analysis · Finite element method · Rock block content · Convexity-concavity feature

1 Introduction

Landslides are considered one of the most damaging and dangerous natural disasters worldwide. They frequently occur in mountainous regions, leading to significant economic losses and numerous casualties (Varnes 1984; Bathrellos et al. 2021; Skilodimou and Bathrellos 2021). Assessing landslide risk in these regions is essential. Qualitative methods have been extensively studied to identify high-risk areas, as has been reported

✉ Gyu-Hyun Go
gyuhyungo@kumoh.ac.kr

[1] Department of Civil Engineering, Kumoh National Institute of Technology, Gumi 39177, Gyeongbuk, Korea

Published online: 16 July 2024

in many previous studies (Kanungo et al. 2013; Bathrellos et al. 2017; Karpouza et al. 2021). Additionally, quantitative methods, based on advancements in computer science and enhanced by field investigations, laboratory testing, and numerical simulations, have been developed to improve the reliability of landslide risk assessments, particularly in geologically complex regions such as soil-rock mixture slopes.

Soil-rock mixture (SRM) represents a type of geomaterial characterized by intense heterogeneity, comprising high-strength rock blocks of varying sizes embedded within a low-strength soil matrix (Medley and Sanz Rehermann 2004; Xu et al. 2008; Wang et al. 2021a, b). Research by Xu et al. (2011) and Coli et al. (2012) explored the spatial distribution of rock inclusions in SRM slopes. Additionally, numerous studies have examined experimental aspects, describing characteristics such as composition, compactness, and strength, to investigate the properties of SRM (Kokusho et al. 2004; Simoni and Houlsby 2006; Zhang et al. 2016; Wei et al. 2018; Wang et al. 2021a, b). Recently, Khorasani et al. (2019) used a tilt-table apparatus to test physical models and assess the stability of SRM slopes with varying rock contents at a laboratory scale. Furthermore, to explore the dynamic characteristics and failure modes of an accumulation body slope (a type of soil–rock mixture slope) due to underground vibration, a large-scale shaking table model test (scale 1:16) was conducted using a specific accumulation body slope as the prototype (Xinglong et al. 2024). Although these experiments have successfully elucidated the mechanical and physical characteristics of SRM, they are limited by high costs and the lack of large-scale testing equipment. Consequently, numerical methods, extensively employed in geotechnical engineering, offer an effective alternative approach.

A common technique involves creating the SRM slope models based on digital image processing (DIP). Yang et al. (2021) indicated that DIP technology could be used to construct the SRM slope models that accurately replicate the structure of rock blocks in soil. They applied the strength reduction numerical manifold method (SRNMM) to calculate the safety factors of the SRM slope. In another approach using the random generation method (RGM), Lianheng et al. (2021) proposed a random generation method of SRM based on DIP to create a substantial number of polygon blocks analogous to real rock blocks. In their study, a library of rocks was established, and SRM slopes were constructed by randomly selecting rock blocks from the library. Subsequently, the finite difference method (FDM) was used to assess the effects of rock block content and its size distribution on slope stability and plastic zone expansion. They indicated that the stability of the SRM slope improved with an increase in rock block content and a more broken plastic zone. A similar technique for creating SRM slope models combined with the finite element method (FEM) to investigate the stability of SRM slopes was proposed by Zhongfeng et al. (2021). For a more accurate understanding of the failure mechanisms related to the large deformation of SRM slopes, Zhao et al. (2022) introduced a new technique: establishing a material point method (MPM) model with the DIP technique. The results revealed that the rock content, rock size, and spatial distribution significantly affected the potential sliding surface of the SRM slopes.

Another effective approach involves constructing SRM slope models from randomly shaped rock blocks using random sequential addition (RSA). Liu et al. (2020a, b) conducted a series of numerical analyses with the FDM to examine the impacts of rock block features, such as the number of edges, size, and inclination, on the stability of SRM slopes. Similarly, other studies have applied random models with rock blocks assumed to have regular shapes, such as circular or elliptical (Napoli et al. 2018, 2021; Huang et al. 2021). Lu et al. (2017) proposed a methodology for generating random rock block shapes, opting for octagons created from basic elements in PFC2D rather than conventional elliptical rock shapes. Further research by Lu

et al. (2018) assessed how rock block morphology influences the mechanical behaviors of clay-rock mixture slopes. Their findings suggested that rock content below 60% could detrimentally impact slope stability, whereas content exceeding 60% substantially enhanced the factor of safety (*FOS*). Yu et al. (2023) reported similar findings when analyzing SRM slope models using the discrete element method (DEM), where a rock-template library was generated using a random aggregate structure (RAS) to establish the SRM slope. Meanwhile, Li et al. (2022) found that the stability of SRM slopes was significantly influenced by the size of the rocks when the rock block content ranged from 5 to 30%, with rock block size having both positive and negative effects on stability. However, these SRM models, which depicted rock blocks as convex polygons, overlooked the degree of convexity-concavity, potentially omitting features more representative of actual rock blocks. Furthermore, the results of previous studies have only been applied to specific cases and certain problem conditions. Therefore, further research is necessary to provide better insights into the evaluation of SRM slope stability.

This study proposes a new approach for randomly generating SRM slope models based on the RAS method and analyzes their stability using the finite element method in ABAQUS. The new method improves the overlap-checking technique, implemented through a Python script in ABAQUS. Additionally, a strength reduction technique was implemented to calculate the slope safety factor, utilizing the USDFLD subroutine in ABAQUS. The non-convergence criterion and the distribution of the plastic zone were applied to determine the verge of failure and to calculate the *FOS* values of the SRM slopes. The *FOS* value of the homogeneous soil slope was validated and compared with previous studies. Subsequently, a series of numerical modeling studies of SRM slopes were conducted to investigate the influence of rock block content, spatial distribution, and the convexity-concavity features of rock blocks on slope stability and the characteristics of the sliding surface.

2 Methodology

2.1 Strength reduction method in ABAQUS

2.1.1 Determination of the safety factor

The strength reduction method has been commonly used to determine *FOS* values for slopes in geotechnical engineering. The *FOS* is defined as the ratio of the initial shear strength parameters to those in the critical equilibrium state (Zienkiewicz et al. 1975; Matsui and San1992; Zheng et al. 2005). The *FOS* is determined as follows:

$$c_f = \frac{c}{FOS},\ \tan\phi_f = \frac{\tan\phi}{FOS} \tag{1}$$

where c and ϕ represent shear strength, and c_f and ϕ_f are the strength parameters when a slope is on the verge of failure.

To conduct the strength reduction technique, a set of elastic-perfectly plastic are computed with i-th shear strength parameters, c_i, and ϕ_i to calculate the *FOS* value

$$c_i = \frac{c}{FOS^i},\ \tan\phi_i = \frac{\tan\phi}{FOS^i} \tag{2}$$

where FOS^i is the i-th shear strength reduction factor.

FOS represents the value of FOS^i at the critical equilibrium state, marking the verge of slope failure. However, various criteria have been used to determine the failure thresholds. Griffiths and Lane (1999) proposed the non-convergence option as an appropriate indicator when no stress distribution can simultaneously satisfy both the global equilibrium and the Mohr–Coulomb failure criterion. Moreover, a significant increase in the nodal displacements within the mesh was observed. Similarly, Korpouza et al. (2021) and Chen et al. (2023) employed a comparable approach for determining the FOS value. Zheng et al. (2005) introduced a criterion based on the distribution of plastic zones, where the plastic zones enclosing the critical zone were connected and passed through the toe to the top of the slope. This moment was used to delineate the verge of failure using a visualization technique. In this study, to enhance the reliability of determining the FOS value, a combination of criteria was applied, including methods based on non-convergence calculations and the criterion based on the distribution of plastic zones, as studied by Yang et al. (2019).

Calculation of the *FOS* value using the strength reduction method in ABAQUS involves three steps: defining the initial state of the soil in the input file prior to analysis, applying a gravity load to establish equilibrium in the initial soil stress field, and implementing the strength reduction technique. For further details, please refer to (Peng et al. 2020).

2.1.2 The ϕ–ν inequality

Zheng et al. (2005) reported that for a geotechnical material satisfying the Mohr–Coulomb failure criterion, the relationship between the internal friction angle, ϕ, and Poisson's ratio, ν can be presented as

$$\sin\phi \geq 1 - 2\nu \tag{3}$$

In the strength reduction method, the shear strength parameters of the soil are adjusted to determine the *FOS* of a slope, while Poisson's ratio is unchanged. This approach leads to the development of spurious plastic zones deep within the slope, arising when the $\phi - \nu$ inequality is not satisfied at sufficiently large FOS^i values. A solution to this problem is that Poisson's ratio also changes during strength reduction, as discussed in the literature proposed by Zheng et al. (2005) and Yang et al. (2019, 2021, 2023).

2.1.3 Implementation strength reduction method and the ϕ–ν inequality

ABAQUS, a finite element software package, offers various user subroutines written in FORTRAN. The USDFLD user subroutine is used to define the field variables at a material point and express them as functions of time or any available material point quantities in the output variable table. This subroutine is called at all material points of the elements for which the material is defined and encompasses user-defined field variables. In a recent study by Liu and Su (2023), the FEM for reducing the double strength parameters based on variations in soil water content was applied to analyze the stability of a slope using the USDFLD user-defined subroutine in ABAQUS. In this study, the USDFLD user subroutine within the ABAQUS finite element software was developed to synchronously execute the shear strength parameters and Poisson's ratio at all material points of the elements at the start of each increment. The strength reduction technique modifies the field variable from an initial value (f_0=0.8). Additionally, the field variables are automatically adjusted based on the time step proposed by the calculation process in ABAQUS/Standard,

with a minimum timestep (Δt_{min}) of 10^{-5} s. Figure 1 illustrates a flowchart depicting the implementation of the USDFLD subroutine in ABAQUS.

2.2 Generation of soil-rock mixture slope

2.2.1 Rock block generation

Randomly shaped rock blocks, such as convex polygons, can be generated based on a set of vertices (Xu et al. 2016). Another approach, based on random radii and angles

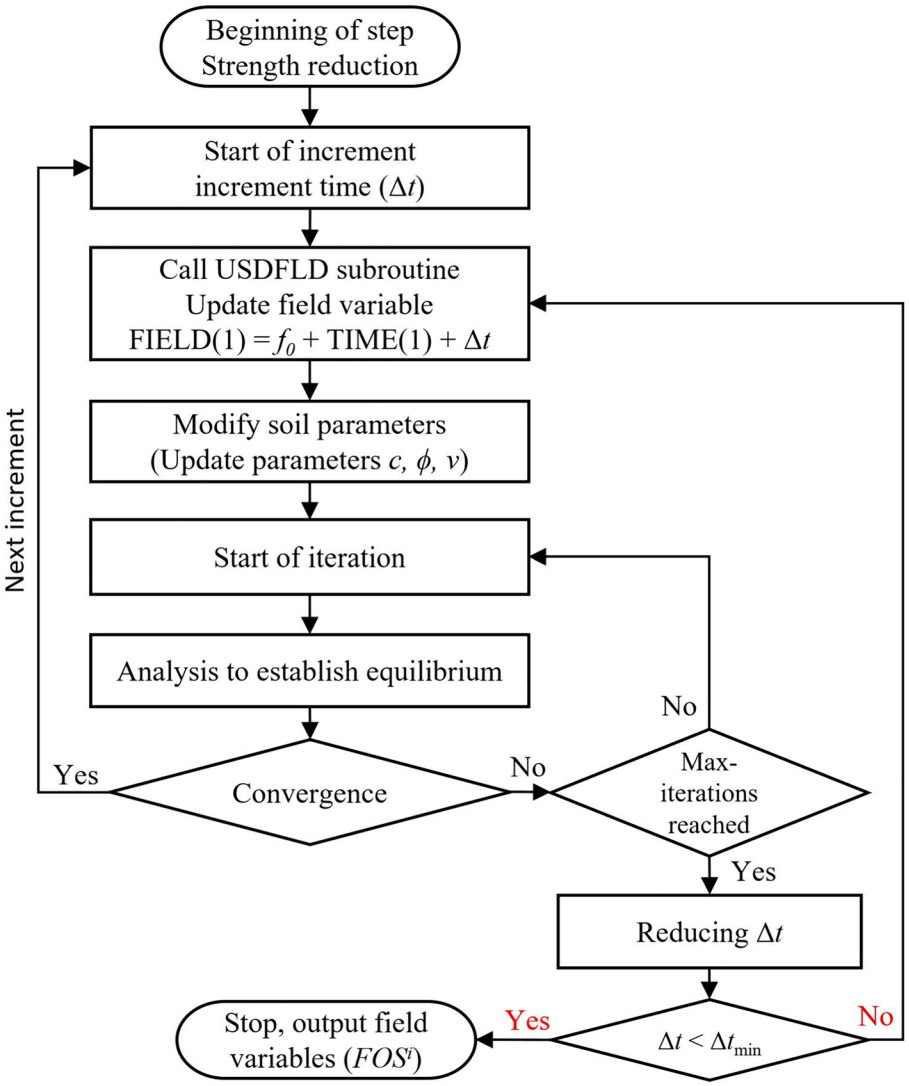

Fig. 1 Flowchart for the implementation of USDFLD Subroutine in ABAQUS

in polar coordinates, provides more parameters to adjust the rock block shape and can create rock blocks with nonconvex polygons, which may be more consistent with the actual rock block shape, as shown in Fig. 2 (Wang et al. 1999; Meng et al. 2018; Yu et al. 2023). In this study, the random aggregate structure method proposed by Wang et al. (1999) was used to generate rock blocks. The shape of the rock block is modeled as an n-vertex polygon, characterized by sequences of polar radii $\{r_1 \ldots r_i, \ldots r_n\}$ and polar angles $\{\theta_1 \ldots \theta_i, \ldots \theta_n\}$ for each vertex. The series of r_i values are assumed to be uniformly distributed around a mean value, r_o, ranging from $(r_o—\Delta r)$ *to* $(r_o + \Delta r)$. This can be described as follows:

$$r_i = r_0 + (2.\zeta - 1).\Delta r \tag{4}$$

where ζ is a random number between [0, 1], and Δr is the amplitude of change of the polar radius. As Δr increases, the convexity–concavity feature of the rock blocks becomes more pronounced. Therefore, $\Delta r/r_0$ is considered a shape parameter in this study, used to describe the convexity–concavity feature of the rock blocks.

The random angle i-th, $\Delta\theta_i$ is determined as the difference between the polar angle of the two adjacent vertices ($\Delta\theta_i = \theta_{i+1} — \theta_i$) as

$$\Delta\theta_i = \frac{2\pi}{n} + (2\zeta - 1).\delta.\frac{2\pi}{n} \tag{5}$$

where δ is the coefficient of amplification for the random angle, ranging between 0 and 1; the angles become more uniform as δ decreases. To ensure the closure of the polygon, its angles were adjusted as follows:

$$\Delta\bar{\theta}_i = \frac{\Delta\theta_i.2\pi}{\sum_{i=1}^{n}\Delta\theta_i} \tag{6}$$

Thus, the polar angles θ_i of the adjusted polygonal rock block can be determined by the following equation:

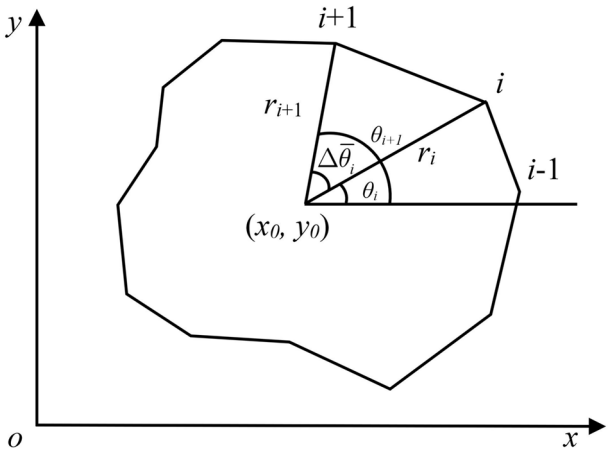

Fig. 2 Generation of random rock block

$$\theta_i = \sum_{j=1}^{i} \Delta\overline{\theta}_j \tag{7}$$

The coordinates of the vertices of randomly generated rock blocks are given in polar coordinates. These can be converted into Cartesian coordinates, and the area of the rock blocks is expressed by the following equations:

$$\begin{cases} x_i = x_0 + r_i.\cos\theta_i \\ y_i = y_0 + r_i.\sin\theta_i \end{cases} \tag{8}$$

$$A_i = \sum_{i=1}^{n-1} \frac{1}{2} r_i r_{i+1} \sin\Delta\overline{\theta}_i \tag{9}$$

where (x_0, y_0) is the central coordinate of the rock block, and (x_i,y_i) is the coordinate of the i-th vertex of the rock block.

The number of edges for each rock block (n) was determined under the assumption that larger rock blocks tend to have more edges, and vice versa, as proposed by Cheng et al. (2023). In this study, rock blocks had 5 to 15 edges.

2.2.2 Location of rock blocks

Due to the high degree of randomness of the rock blocks on the SRM slope, the center positions of the rock blocks are also randomly distributed within the model generation domain. It is assumed that distribution is uniform and random across the entire area of the model domain. When the rock block is placed in the slope section, its center position is defined by the coordinates (x_0, y_0) in a Cartesian x–y coordinate system, and the coordinates of the center position can be determined as

$$\begin{cases} x_0 = x_{\min} + \eta_1.(x_{\max} - x_{\min}) \\ y_0 = y_{\min} + \eta_2.(y_{\max} - y_{\min}) \end{cases} \tag{10}$$

where x_{min}, x_{max}, y_{min}, and y_{max} are the minimum and maximum x– and y– coordinates of the model domain, respectively, η_1 and η_2 are two independent random values uniformly distributed within [0, 1].

In the model generation domain, a rock block is defined by its central coordinate position, polar radii, and polar angles. To judge the invasion of new rock blocks with previously existing ones, Xu et al. (2016) proposed a method to determine the intersection between convex polygonal blocks using the angle criterion, area criterion, and edges intersect. Wang et al. (1999), Meng et al. (2018), and Lianheng et al. (2021) examined the overlap between rock blocks by constructing a bounding box, which was the smallest rectangle that can surround an object for each rock block. In this study, an algorithm for detecting intersections is developed as follows:

First, (x_i, y_i) are the central coordinates of the i–th rock block, and $r_{i,\max}$ is its maximum radius. Assume that the j–th is one of the previously generated i–1 rock blocks with central coordinates (x_j, y_j), and $r_{j,\max}$ is its maximum radius. The distance d between the centers of the two rock blocks is calculated as follows:

$$d = \sqrt{(x_i - x_j)^2 + (y_i - y_j)^2} \tag{11}$$

If $d > r_{i,\max} + r_{j,\max}$, then there is no intersection between the i-th and j–th rock blocks, and it will turn to the next step, which is to detect the intersection between the i-th and $j+1$–th rock blocks.

Second, if $d \le r_{i,\max} + r_{j,\max}$, indicating that two rock blocks intersect, there will be at least one intersection between the edges of two rock blocks, and their corresponding coordinates are shown in Fig. 3a. The coordinates of the intersection satisfy the following conditions:

$$\begin{cases} \min(x_i, x_{i+1}) \le x \le \max(x_i, x_{i+1}) \\ \min(x_j, x_{j+1}) \le x \le \max(x_j, x_{j+1}) \\ \min(y_i, y_{i+1}) \le y \le \max(y_i, y_{i+1}) \\ \min(y_j, y_{j+1}) \le y \le \max(y_j, y_{j+1}) \end{cases} \tag{12}$$

If no intersection is detected by the above steps, another type of intersection may exist where the vertices of one rock block are included by another. Assume that all vertices of rock block j are within rock block i. There will be a point of intersection of the two lines determined as follows: the first line is defined by the two centers of the rock blocks, and the second line is defined by the edge of the j rock block, as shown in Fig. 3b. The coordinates of the intersection satisfy the following conditions:

$$\begin{cases} \min(x_{0i}, x) \le x_{0j} \le \max(x_{0i}, x) \\ \min(y_{0i}, y) \le y_{0j} \le \max(y_{0i}, y) \\ \min(x_i, x_{i+1}) \le x \le \max(x_i, x_{i+1}) \\ \min(y_i, y_{i+1}) \le y \le \max(y_i, y_{i+1}) \end{cases} \tag{13}$$

2.2.3 Size distribution of rock blocks

The size distribution of rock blocks, d, can be taken as 0.05 – 0.75 L_c, where L_c is the SRM slope height (Napoli et al. 2018; Zhao et al. 2022). The height of the SRM slope is 10 m, thus a reasonable value of d is between 0.5 and 7.5 m. In the present study, the size distribution of the rock blocks is described by the equivalent diameter, which is defined as the diameter of a circular rock block that has the same area as a polygonal rock block (Lianheng et al. 2021).

The process of generating a rock block with an equivalent diameter equal to a preset value (d) involves setting the average radius of the rock block to $r_0 = d/2$ with the calculated area A_i, as outlined in Sect. 2.2.1. However, the equivalent diameter of this rock block often does not equal d. Therefore, the size of the rock block is adjusted to ensure that its equivalent diameter equals d while the shape remains unchanged. The adjustment coefficient and the polar $r - \theta$ coordinates of the polygonal rock block after change can be calculated as

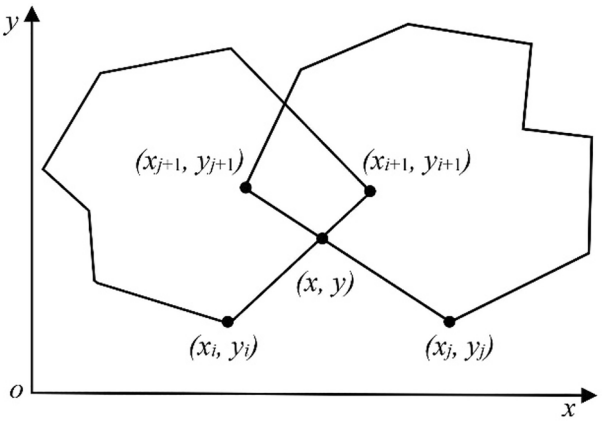

(a) Intersection between polygonal blocks

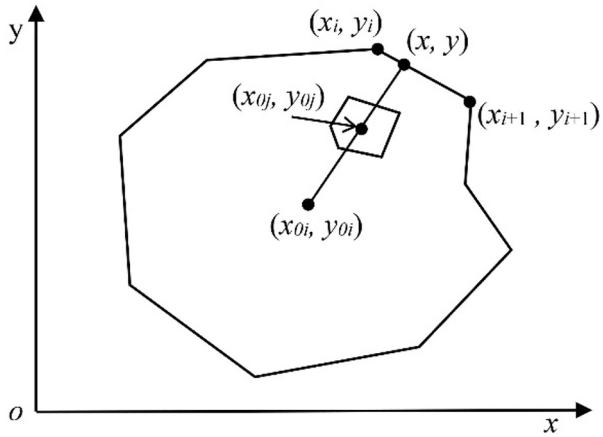

(b) Vertices of polygonal block are included in the other

Fig. 3 The condition of overlapping between two polygonal blocks

$$\alpha = \frac{d}{2\sqrt{A_i/\pi}} \tag{14}$$

$$\begin{aligned} r_i' &= \alpha . r_i \\ \theta_i' &= \theta_i \end{aligned} \tag{15}$$

2.2.4 SRM model generation

The SRM slope model was generated by placing rock blocks with a specific size distribution within the model domain. To minimize the overlap between rock blocks, placement was performed by size group, from largest to smallest. Additionally, the minimum distance between two rock blocks was set using the coefficient γ, whereby

the polar radius of the new polygonal rock block was enlarged to γ times its original size during the detection of intersections between two rock blocks (Wang et al. 1999). A Python script was developed to generate the model geometry of the SRM slope in ABAQUS. A flowchart of the random generation of the SRM slope is shown in Fig. 4.

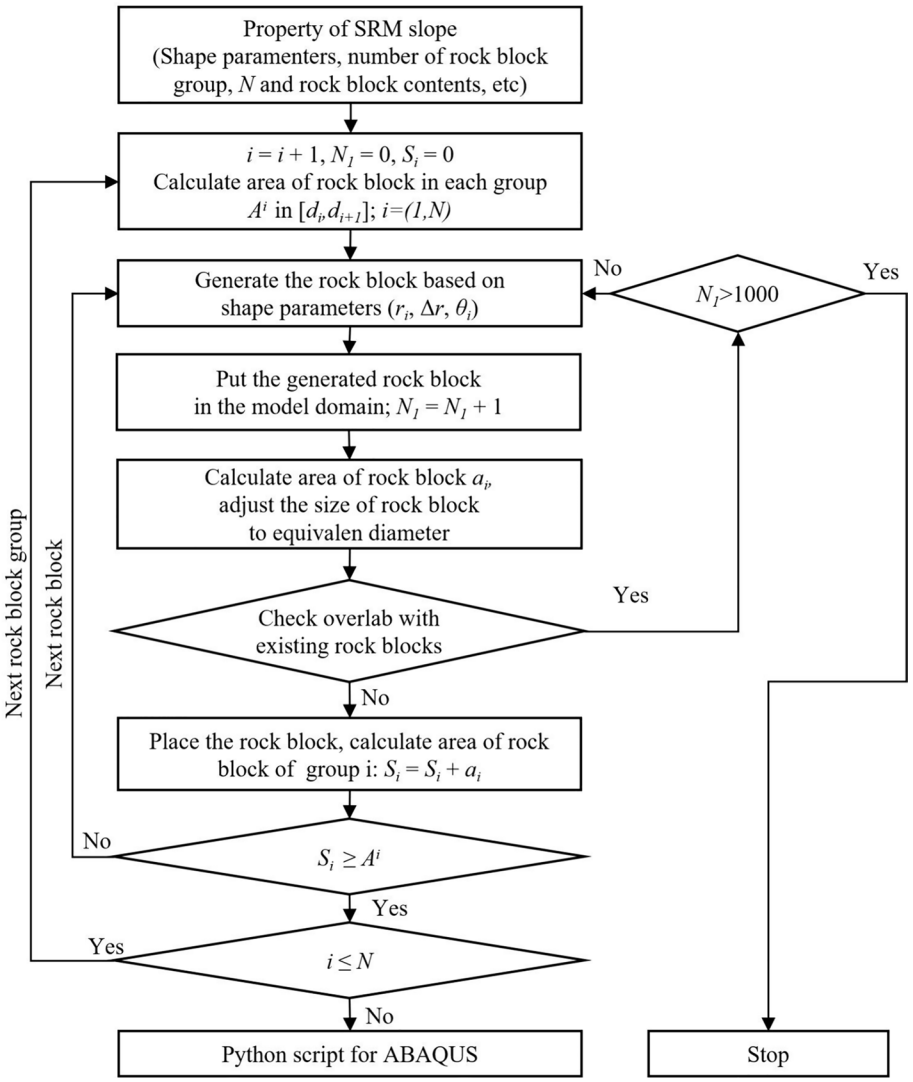

Fig. 4 Flowchart outlining the steps for generating a model for SRM slope

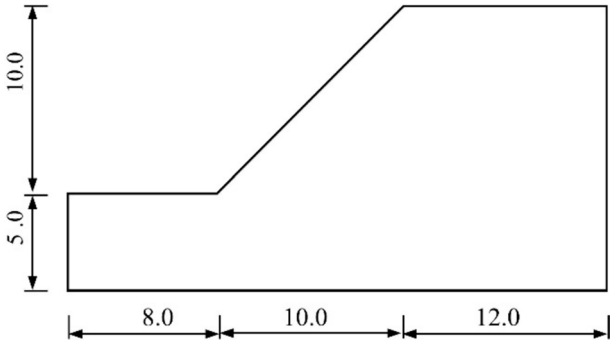

Fig. 5 Geometry of the slope model (unit: m)

Table 1 Properties of materials used in stability analysis

Material	Density (kg/m^3)	Young's modulus (MPa)	Poisson's ratio	Friction angle (°)	Cohesion (KPa)
Soil	2,000	200	0.35	20	12.38

3 Results

3.1 Stability analysis of homogeneous soil slope

To validate the computational results from ABAQUS and determine the appropriate element mesh for the research models, a specific geometric dimension of the homogeneous soil slope was selected, guided by previous studies (Chen 1975; Zheng et al. 2005; Sun et al. 2020). Furthermore, this study focuses on examining the effects of the content, shape, and spatial distribution of rock block on the stability of SRM slopes. Accordingly, a geometric model was used, as depicted in Fig. 5. The bottom boundary of the model was fixed, and roller conditions were applied on both sides. The slope was subjected only to the self-weight of the soil. The Mohr–Coulomb elastic–plastic model with the non-associated flow rule was used in ABAQUS, with parameters listed in Table 1. The elements were set as four-node bilinear plane strain quadrilaterals (CPE4). Mesh convergence was investigated with approximate global element sizes of 0.5, 0.4, 0.3, and 0.2 m. The ABAQUS results indicated that the *FOS* was 0.989 for the approximate global size of 0.4 and 0.5 m, and 0.979 for the approximate global size of 0.3 and 0.2 m. The analysis revealed that the differences in *FOS* for the approximate global sizes ranging from 0.2 to 0.5 m were insignificant; therefore, a global size of 0.2 m was applied for meshing to all models for this study. The equivalent plastic strain contours of the homogeneous soil slope with the approximate global size of 0.2 m are illustrated in Fig. 6.

Under the same conditions for a homogeneous soil slope using the limit analysis method, a safety factor of 1.0 was determined by Chen (1975), while Zheng et al. (2005) obtained a *FOS* of 1.06 via the FEM. Another study by Sun et al. (2020) calculated the *FOS* of 0.99 using the virtual element method. The *FOS* values in this study were very close to those reported in previous studies (Table 2).

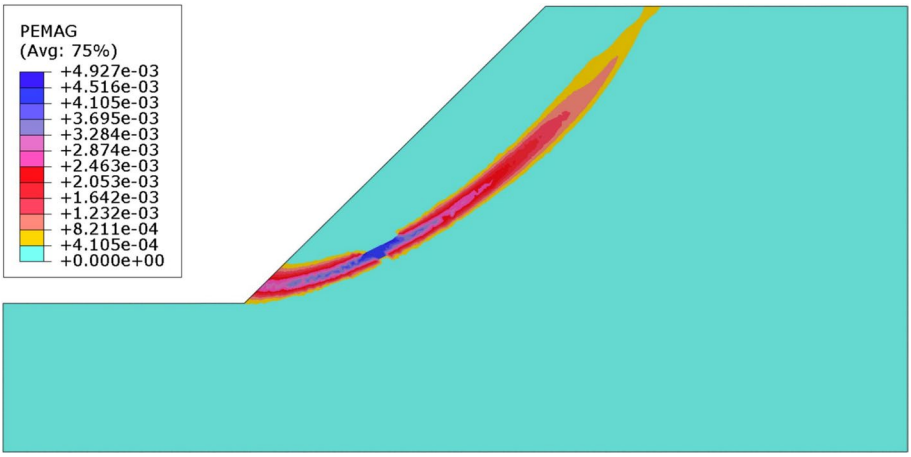

Fig. 6 Equivalent plastic strain contours in homogenous soil slope

Table 2 Comparison of *FOS* value in this study with previous studies

Previous studies	*FOS*	Deviation (%)
Chen (1975)	1.000	− 2.15
Zheng et al. (2005)	1.060	− 8.27
Sun et al. (2020)	0.990	− 1.12

Table 3 Properties of materials used in stability analysis

Material	Density (kg/m^3)	Young's modulus (MPa)	Poisson's ratio	Friction angle (^{o})	Cohesion (KPa)
Soil	2,000	200	0.35	20	12.38
Rock	2,410	20,000	0.2	42	900

3.2 Stability analysis of soil-rock mixture slope

3.2.1 Influence of rock block content on the stability of SRM slope

This section discusses the influence of the rock block content at varying percentages (10, 20, 30, 40, and 50%). Table 3 provides a detailed distribution of rock block sizes based on their equivalent diameter. The properties of the materials used in the stability analysis are listed in Table 4. Additionally, 15 SRM slopes were randomly generated for each rock block content to conduct a statistical investigation. The statistical results of *FOS* values for the SRM slopes with different rock block contents are presented in Table 5, and the box diagram is illustrated in Fig. 9 (detailed in Table 6). The equivalent plastic strain contours of the SRM slopes for rock block contents of 10% and 50%, along with their corresponding *FOS* values, are shown in Figs. 7 and 8.

Table 4 Rock block sizes distribution with different contents and shape parameters of rock blocks

Equivalent diameter (m)	Ratio (%)	Rock block contents	Shape parameter
2.0–2.3	10	10%, 20%, 30%, 40%, 50%	$\Delta r/r_0 = 0.2$
1.7–2.0	24		
1.4–1.7	25		
1.1–1.4	18		
0.8–1.1	12		
0.5–0.8	11		

Table 5 The statistical indices of *FOS* value for SRM slopes with different rock block contents

Rock content (%)	Mini-value *FOS*	Maxi-value *FOS*	*FOS* mean value	Standard deviation
0	0.979	0.979	0.979	–
10	0.962	1.099	1.016	0.044
20	0.955	1.187	1.057	0.061
30	1.089	1.298	1.172	0.071
40	1.087	1.475	1.311	0.109
50	1.436	1.802	1.666	0.108
Rate of change	46.68%	84.07%	70.13%	–

As shown in Fig. 7, four SRM slopes with a rock block content of 10% exhibited *FOS* values lower than those observed for the homogeneous soil slope. This trend also persisted in the two SRM slopes with a rock block content of 20%, as detailed in Table 6. This phenomenon occurred when the rock block content in an SRM slope was low; the

Table 6 The results of *FOS* value for 75 SRM slopes with different rock block contents

	Rock block contents				
	10%	20%	30%	40%	50%
FOS	0.962	0.959	1.105	1.212	1.595
	0.981	1.081	1.114	1.291	1.665
	1.028	1.079	1.209	1.274	1.785
	0.990	1.081	1.259	1.467	1.700
	0.997	1.063	1.203	1.324	1.612
	1.027	1.088	1.103	1.406	1.796
	0.966	1.075	1.164	1.228	1.579
	1.038	1.084	1.265	1.338	1.608
	1.076	1.187	1.184	1.204	1.694
	1.043	1.074	1.089	1.239	1.719
	0.973	0.981	1.141	1.087	1.513
	1.028	1.040	1.097	1.437	1.774
	0.965	1.109	1.104	1.298	1.802
	1.099	0.955	1.298	1.380	1.705
	1.067	1.004	1.242	1.475	1.436

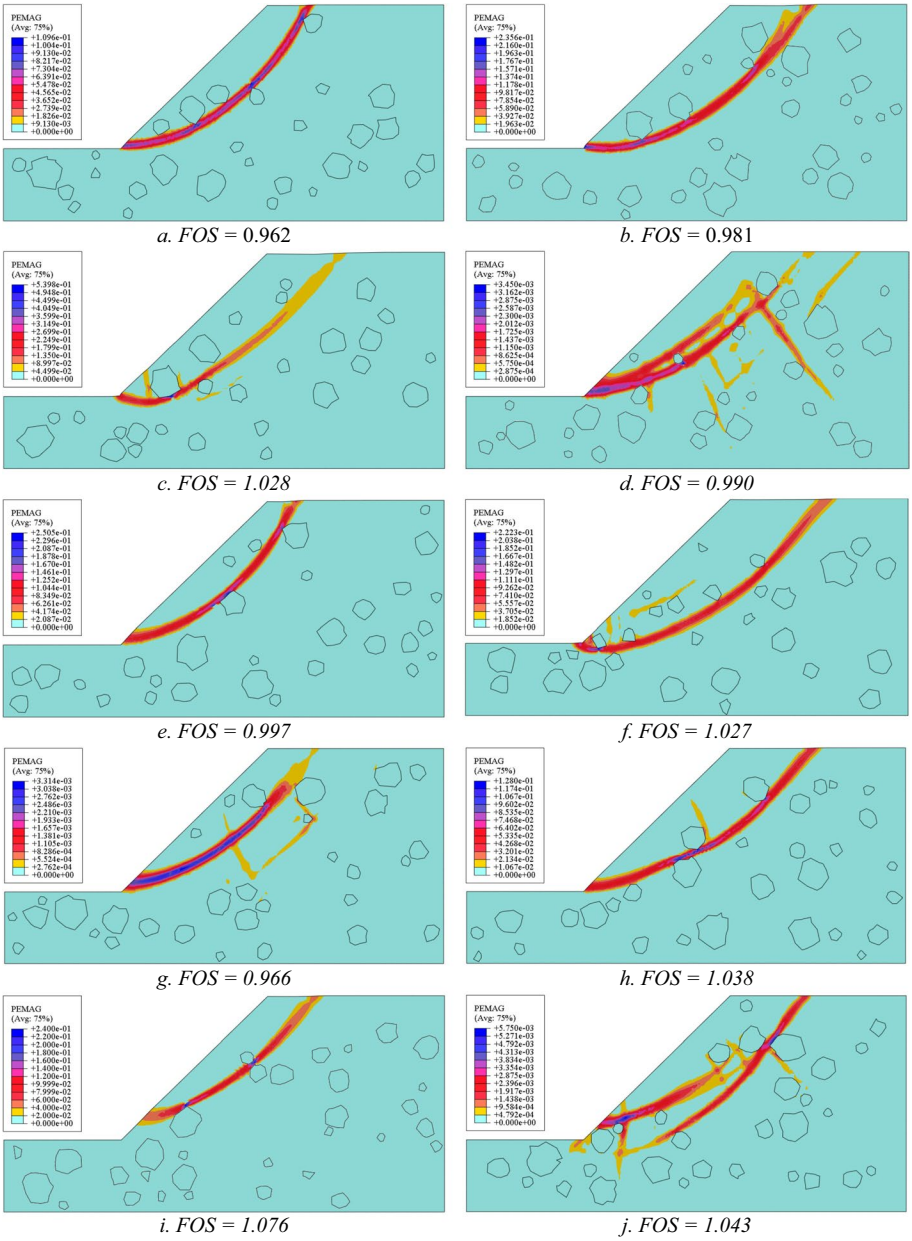

Fig. 7 Equivalent plastic strain contours of 15 SRM slopes with rock block content of 10%

distribution of rock blocks created sufficient space for the plastic zone to develop from the base to the top of the SRM slope without obstruction by high-strength rock blocks. Additionally, the distribution of rock blocks in SRM slopes contributed to an increase in self-weight compared to the homogeneous soil slope, leading to decreased stability.

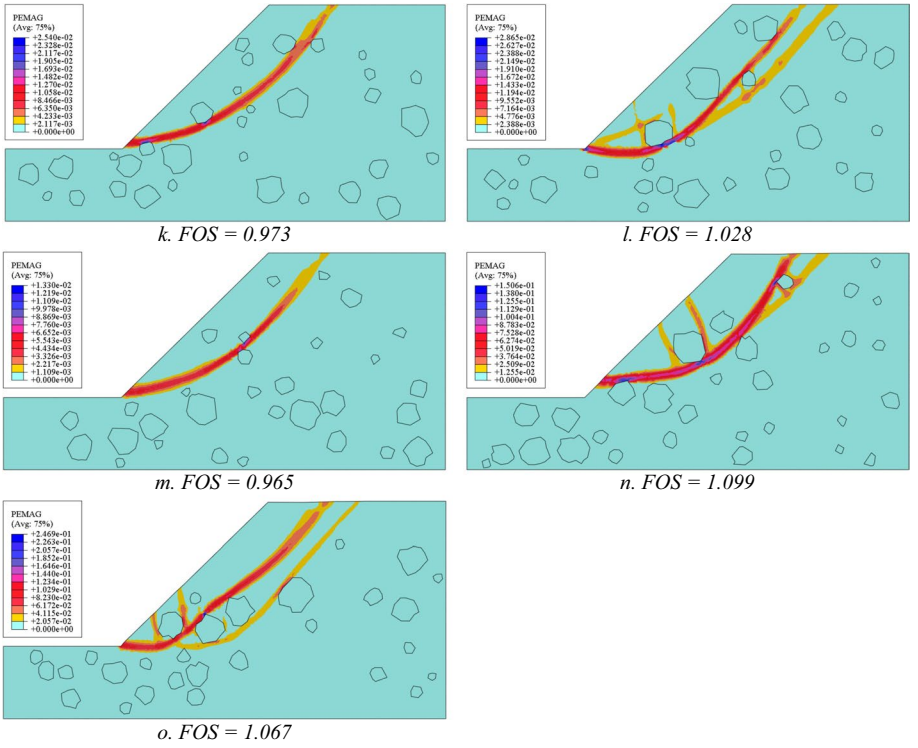

Fig. 7 (continued)

However, this phenomenon did not occur in SRM slopes with rock block contents of 30, 40, and 50% (Fig. 9).

As indicated in Table 6, the statistical analysis of *FOS* values across the 75 SRM slopes for five different rock block contents showed that due to the diverse random distribution of rock blocks, the *FOS* values exhibited discreteness, and the dispersion of these values increased with higher rock block content. The presence of rock blocks in the SRM slope had a significant influence on the failure expansion. The plastic zone in the SRM slope became more complex as the rock block content increased, resulting in multiple sliding zones that represented a combination of various plastic zones, as shown in Fig. 8.

Generally, the presence of rock blocks on a slope improved its stability. As shown in Table 5, when the rock block content was high (30, 40, and 50%), the mean *FOS* value of the SRM slope increased significantly. Specifically, in the SRM slope with a rock block content of 50%, the mean *FOS* value increased by 70.13% compared to that of the homogeneous soil slope. For technical reference, a fitting curve based on the mean value at different rock block contents with a correlation coefficient of the curve greater than 0.98, as shown in Fig. 10.

3.2.2 Influence of rock block shape on the stability of SRM slope

As discussed in Sect. 2.2.1, the convexity-concavity feature of the rock block can be described using the rock block shape parameter $\Delta r/r_0$. In this study, shape parameters

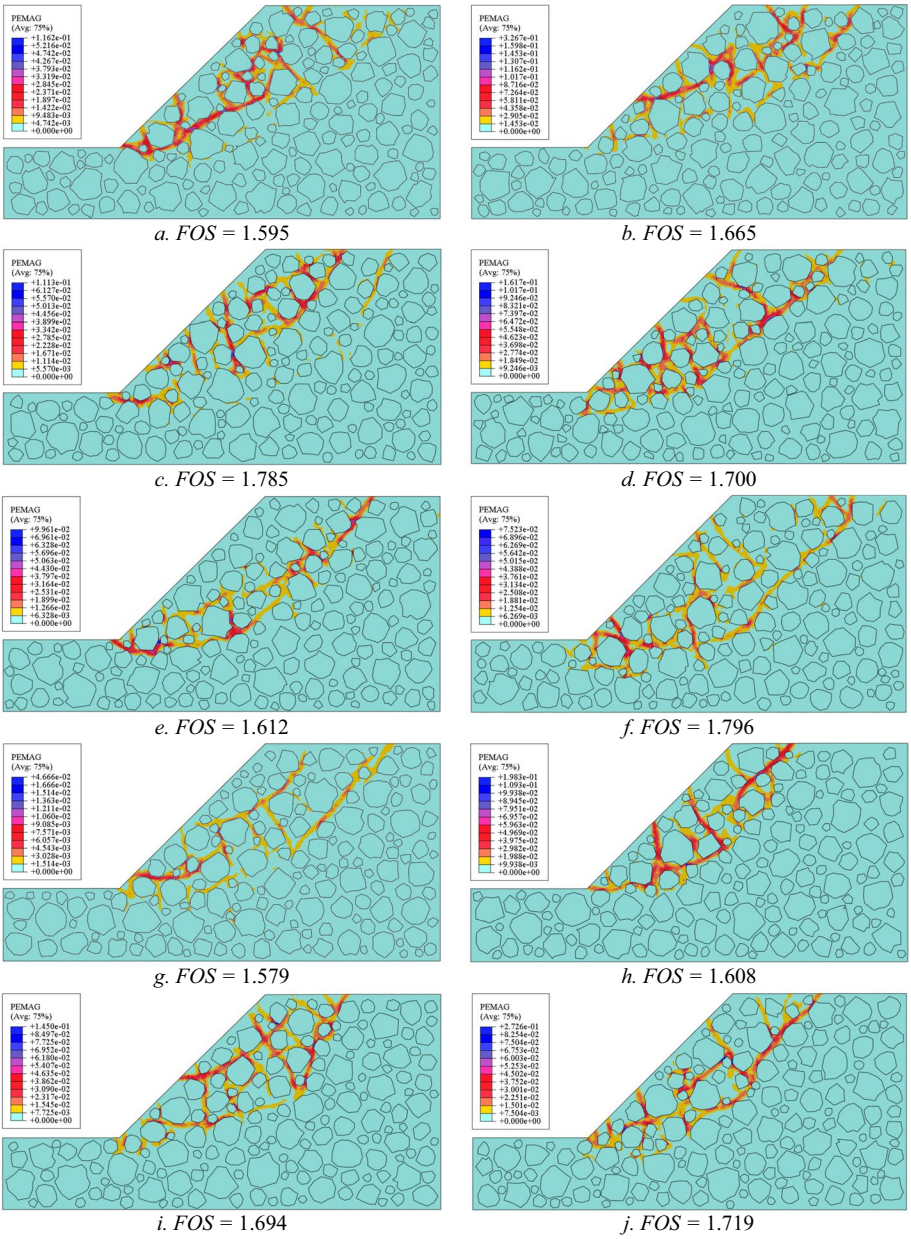

Fig. 8 Equivalent plastic strain contours of 15 SRM slopes with rock block content of 50%

ranging from 0 to 0.4 (specifically, 0, 0.1, 0.2, 0.3, and 0.4) were employed, along with a rock block content of 40%, to consider their influence on the safety factor of the SRM slope. Additionally, the δ parameter was set to 0.5, instead of being randomly assigned values from 0 to 1, as shown in Eq. (5). The statistical results of the *FOS* values for the SRM slopes with different shape parameters are presented in Table 7,

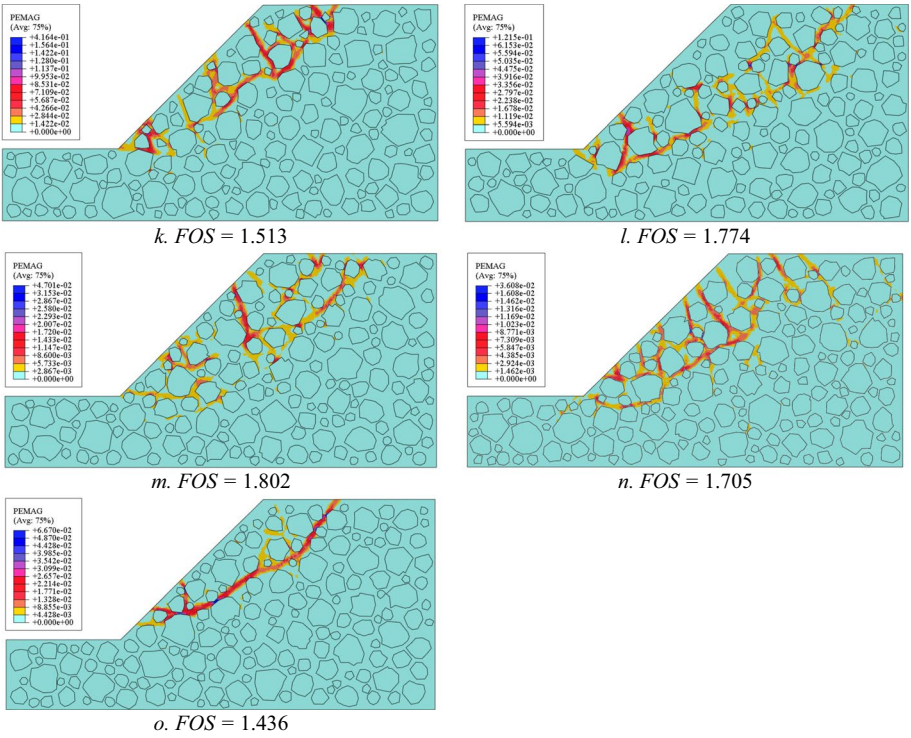

Fig. 8 (continued)

with the corresponding box diagram in Fig. xx13xx (detailed in Table 8). The equivalent plastic strain contours of the SRM slopes for shape parameters of 0 and 0.4, and their corresponding *FOS* values, are illustrated in Figs. 11 and 12.

As observed in Fig. 13, Tables 7 and 8, the *FOS* values exhibited fluctuations as the degree of convexity–concavity of the rock blocks increased, with $\Delta r/r_0$ values of 0, 0.1 and 0.2; however, the mean value did not change significantly. The increasing trend became more clearly apparent only when the $\Delta r/r_0$ values reached 0.3 or 0.4, as reflected in the maximum, minimum, and mean *FOS* values. The results indicate that the degree of convexity–concavity of the rock block improve the stability of the SRM slopes. Specifically, the mean value increased by 14.31% at $\Delta r/r_0 = 0.4$. Additionally, the equivalent plastic strain contours at high shape parameters appeared more complex, as shown in Figs. 11 and 12. The relationship curve between the mean *FOS* values and $\Delta r/r_0$ values, with a correlation coefficient of the curve greater than 0.98, is depicted in Fig. 14.

4 Discussions

The content, shape, and spatial distribution of rock blocks within a slope are critical factors affecting the stability of SRM slopes. Generally, an increase in rock block content is associated with enhanced stability of SRM slopes. This observation is consistent with the

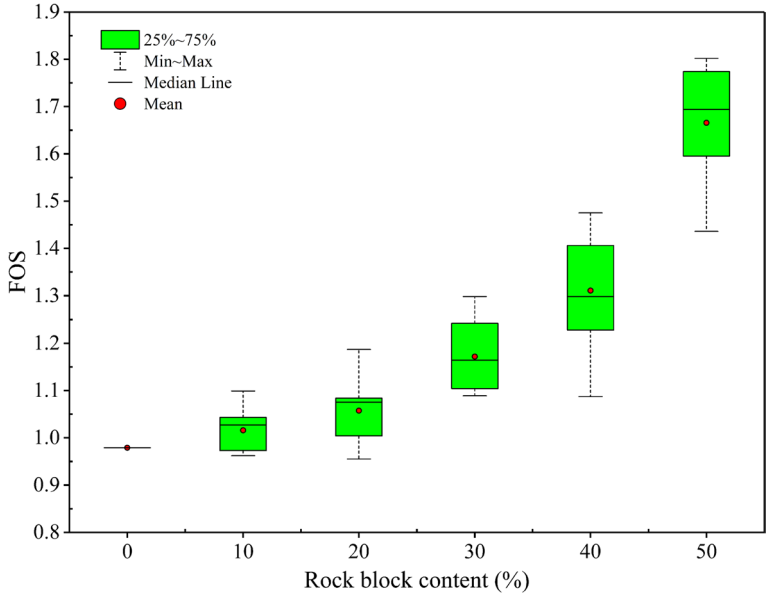

Fig. 9 Box diagram statistical FOS values for SRM slopes with different rock block content

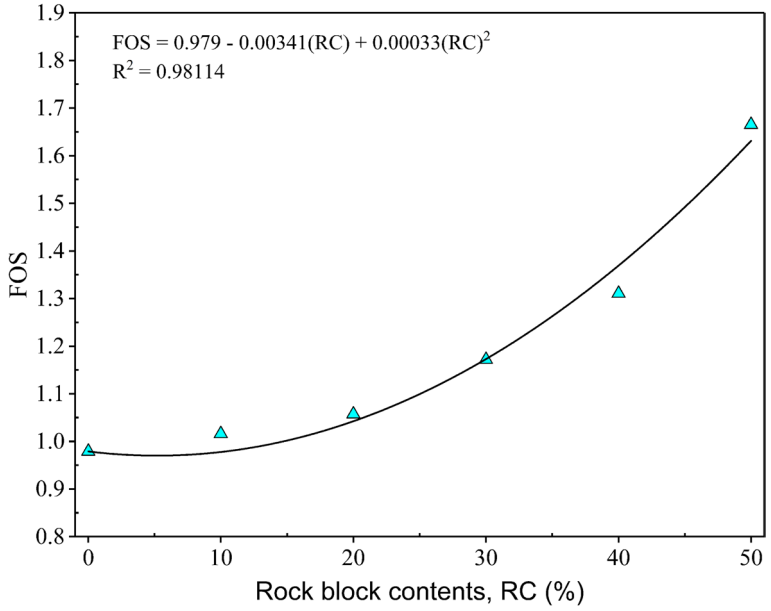

Fig. 10 Relationship between mean FOS and rock block content

results from previously reported studies (Lianheng et al. 2021; Liu et al. 2020a, b; Napoli et al. 2018, 2021). However, slopes with rock block content below 20% may exhibit higher or lower *FOS* compared to those on slopes devoid of rock blocks, highlighting the potential

Table 7 The statistical indices of *FOS* value for SRM slopes with different shape parameters, $\Delta r/r_0$

$\Delta r/r_0$	Minimum value *FOS*	Maximum value *FOS*	*FOS* mean value	Standard deviation
0	1.153	1.403	1.275	0.090
0.1	1.113	1.435	1.295	0.102
0.2	1.143	1.446	1.298	0.088
0.3	1.283	1.470	1.365	0.052
0.4	1.317	1.709	1.457	0.108
Rate of change	14.22%	21.81%	14.31%	–

Table 8 The results of *FOS* value for 75 SRM slopes with different shape parameters, $\Delta r/r_0$

	Shape parameter, Δr/r0				
	0	0.1	0.2	0.3	0.4
FOS	1.382	1.321	1.312	1.405	1.368
	1.213	1.187	1.348	1.470	1.397
	1.265	1.237	1.313	1.365	1.342
	1.179	1.302	1.286	1.356	1.423
	1.165	1.395	1.361	1.454	1.709
	1.153	1.434	1.304	1.365	1.317
	1.394	1.223	1.446	1.360	1.413
	1.224	1.388	1.420	1.362	1.536
	1.227	1.350	1.319	1.382	1.586
	1.305	1.435	1.287	1.283	1.515
	1.389	1.113	1.293	1.403	1.431
	1.356	1.225	1.148	1.342	1.463
	1.267	1.149	1.317	1.301	1.586
	1.203	1.314	1.143	1.315	1.392
	1.403	1.352	1.167	1.318	1.384

adverse impact of sparse rock block distribution on SRM slope stability. Another significant finding of this study is that the convexity-concavity feature of rock blocks can improve the *FOS* of SRM slopes. This enhancement is attributed to the degree of convexity-concavity of the rock blocks, which acts as a barrier to the continuous development of the plastic strain zone on the slope, thereby increasing the *FOS*.

To establish models and analyze the stability of slopes with complex geomaterials, various approaches have been adopted. Napoli et al. (2018, 2021) utilized MATLAB and AutoCAD software to create their models, which were then analyzed using the FEM with the RS2 code from Rocscience. They highlighted the limitations of the traditional Limit Equilibrium Method for predicting the FOS of SRM slopes. Similarly, Liu et al. (2020a, b) developed SRM models using CAD software and analyzed them with the FDM in PLAC3D software. Lu et al. (2018) employed the DEM in PFC2D, which is particularly effective for analyzing large deformations and discontinuous behaviors. However, DEM simulations are computationally demanding and require detailed input about grain properties and interactions, often difficult to obtain from conventional experimental data. Recently, Li et al. (2022) developed a novel method combining Discontinuous Deformation Analysis with

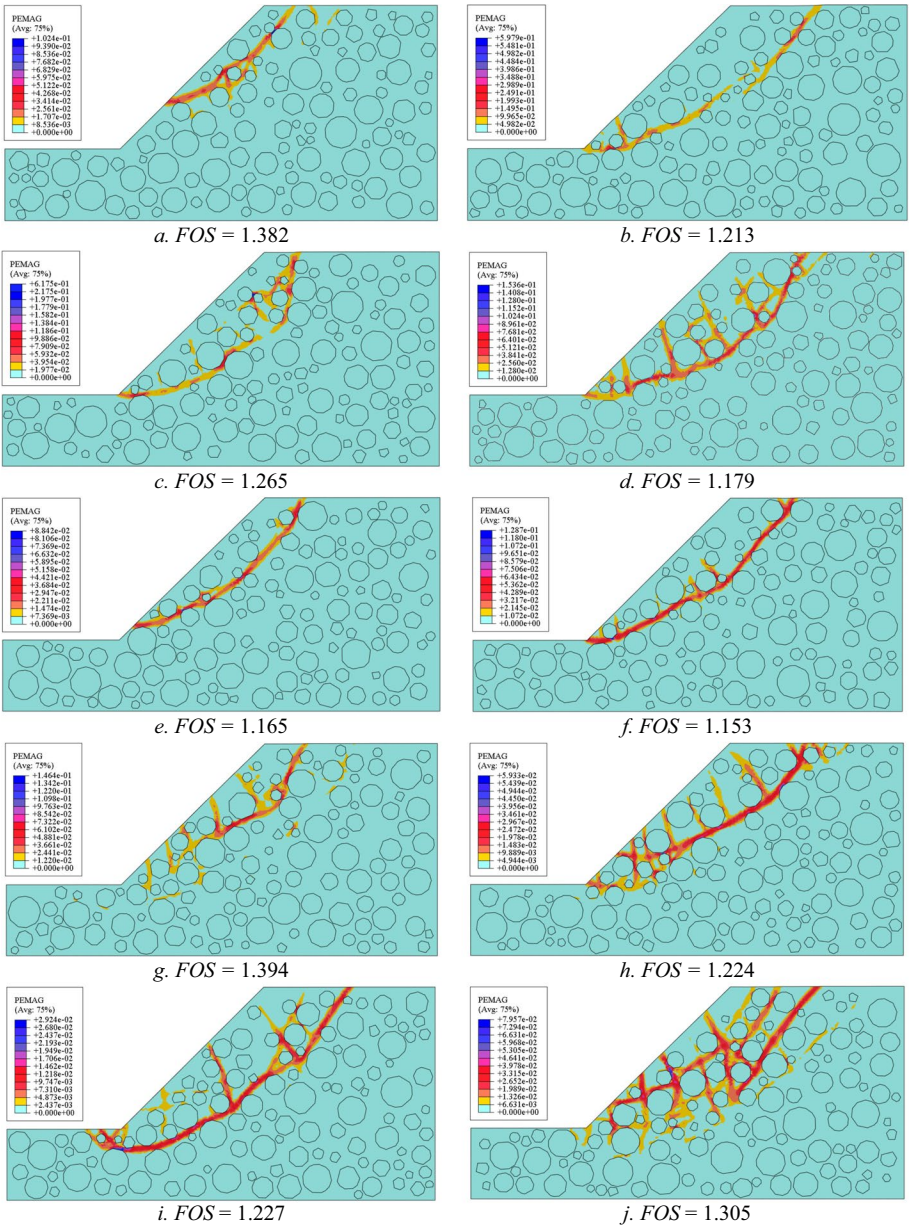

Fig. 11 Equivalent plastic strain contours of 15 SRM slopes with $\Delta r/r_0 = 0$

Smoothed Particle Hydrodynamics (DDA-SPH) for analyzing the stability of SRM slopes. Their study was limited to SRM slopes with rock block contents below 30%, as higher rock mass content significantly increases computational time. In general, while methods such as DEM, DDA-SPH, and the MPM are complex and challenging to apply widely in

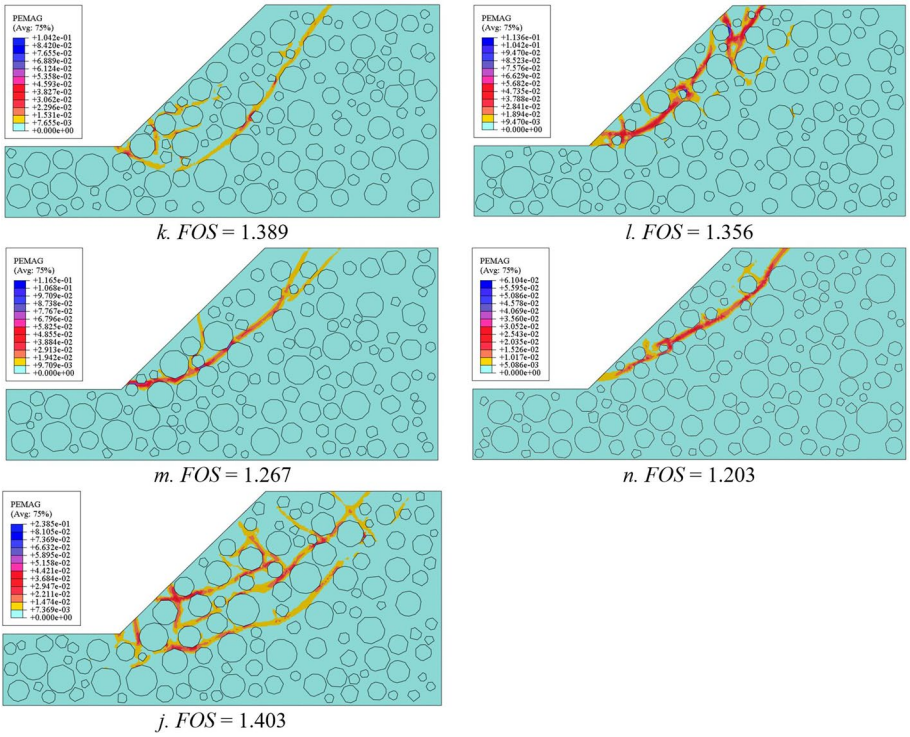

Fig. 11 (continued)

practical design calculation practices, especially when statistical analysis is required, the FEM remains the tool of choice due to its many advantages (Augarde et al. 2021).

ABAQUS software offers significant advantages over conventional FEM software, particularly in the geotechnical field. Its superior capability to handle complex, nonlinear behaviors typical of soil and rock materials renders it invaluable for simulating a broad spectrum of geotechnical problems (Augarde et al. 2021). Additionally, ABAQUS supports robust integration with Python, enabling the automation of modeling and analysis processes. This integration significantly enhances work efficiency, especially when handling multiple or highly complex models. ABAQUS has been widely used in previous research to study slope stability problems (Xiang and Zi-Hang 2017; Dyson and Tolooiyan 2018, 2019; Peng et al. 2020; Liu et al. 2020a, b; Gao et al. 2021; Zhongfeng et al. 2021). In the current work, a novel method for generating random SRM slope models, considering the convexity-concavity feature of rock blocks, is efficiently implemented in ABAQUS using a Python script. This fully automated process simplifies the workflow by eliminating the need for supporting software such as AutoCAD to generate SRM models. Therefore, the use of commercial ABAQUS software not only offers significant advantages but also has the potential to be widely applied in reliably predicting the stability of SRM slopes at a reasonable computational cost.

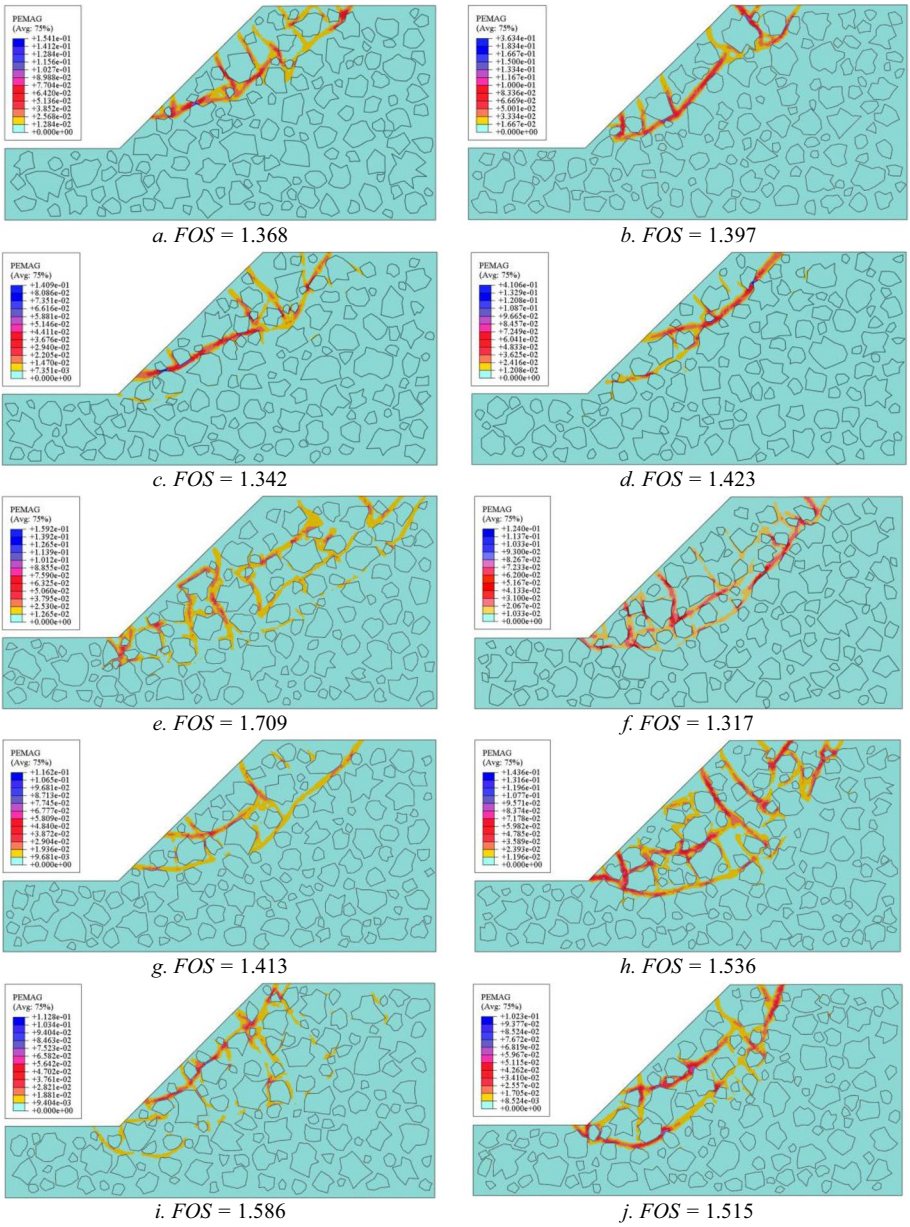

Fig. 12 Equivalent plastic strain contours of 15 SRM slopes with $\Delta r/r_0 = 0.4$

5 Conclusions

This study enhanced a technique using RSA to construct random SRM slope models. The models simulated rock block shapes with varying degrees of convexity-concavity and incorporated various rock block contents for SRM slope stability analysis. Furthermore, a

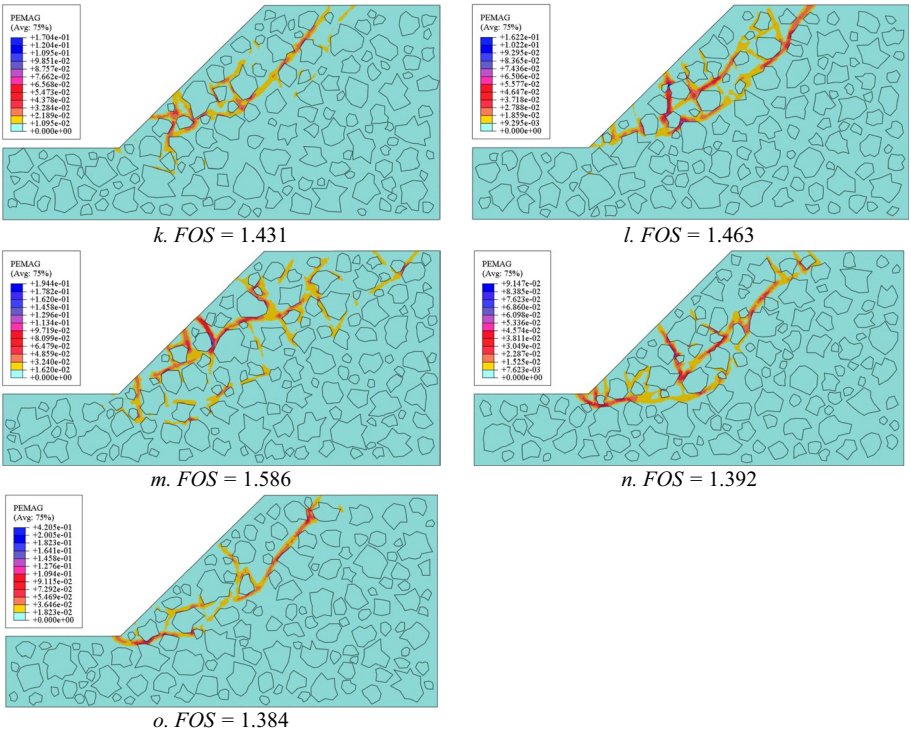

Fig. 12 (continued)

user-defined subroutine was developed within the ABAQUS finite element software to perform soil strength reduction techniques. Subsequently, a series of numerical studies were conducted to assess the influence of the content, spatial distribution, and convexity-concavity features of rock blocks on the stability and failure surface of the SRM slopes. The following main conclusions were drawn:

1. With the same block size distribution, the stability of the SRM slopes can be adversely affected by a low rock block content (10% and 20%), depending on the random location of the rock block within the SRM slope. Conversely, higher rock block content (30, 40, and 50%) positively influences stability, significantly enhancing the *FOS* values compared to those of a homogeneous soil slope.
2. The mean *FOS* value of the SRM slopes rises with increasing rock block content. However, this increasing trend is more clearly observed at higher rock block contents (30, 40, and 50%). Compared to a homogeneous soil slope, the mean *FOS* value of the SRM slope with 50% rock block content increases dramatically by more than 70%. Furthermore, as rock block content increases, the plastic zone becomes more complex, and the FOS values show greater discreteness and dispersion.
3. At the same 40% rock block content in the SRM slopes, the convexity-concavity feature of the rock blocks does not clearly improve stability of the SRM slopes with shape parameters of 0, 0.1, and 0.2. However, with shape parameters of 0.3 and 0.4 for the

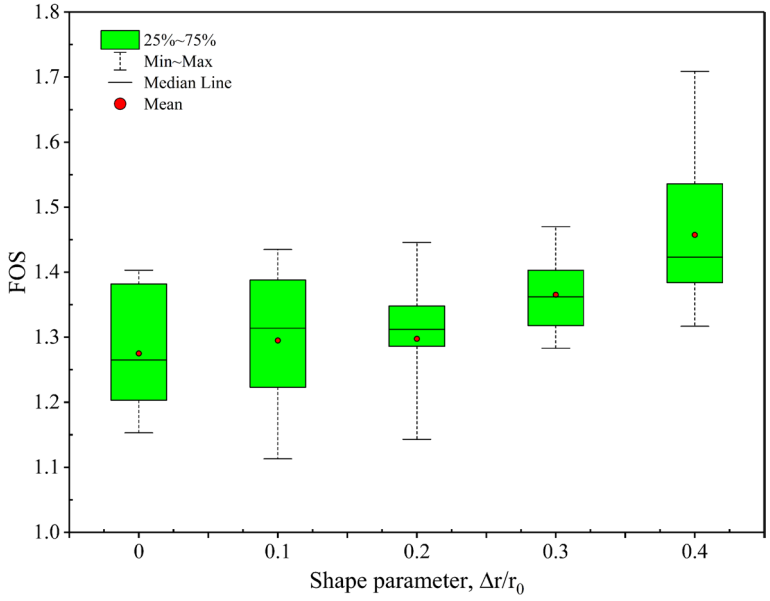

Fig. 13 Box diagram statistical *FOS* values for SRM slopes with different shape parameters, $\Delta r/r_0$

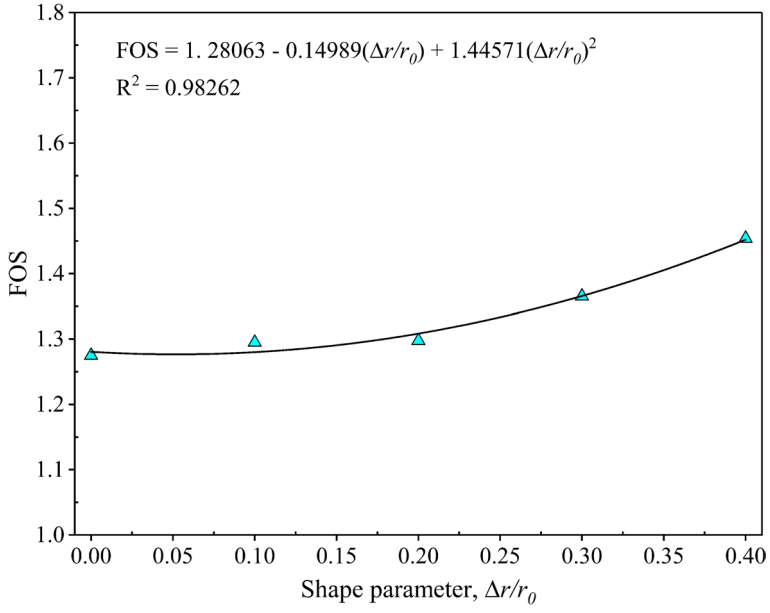

Fig. 14 Relationship between mean *FOS* for SRM slopes with shape parameter, $\Delta r/r_0$

rock blocks positively affect the stability of the SRM slopes, and the mean *FOS* value increases by more than 14% compared with the case of a shape parameter of 0. In addition, the complexity of the failure surface increases with the shape parameters.

Acknowledgements This work was supported by the National Research Foundation of Korea (NRF) grant funded by the Korea government (MSIT) (No. 2022R1C1C1006507).

Author's contribution Cao Van Hoa: Methodology, Numerical analysis, Investigation, Writing—original draft. Gyu-Hyun Go: Conceptualization, Methodology, Resources, Supervision, Funding acquisition, Writing—review & editing.

Declarations

Conflict of interest The authors declare that they have no known competing financial interests or personal relationships that could have appeared to influence the work reported in this paper.

Ethical approval The authors have no conficts of interest to declare that are relevant to the content of this paper.

References

Augarde CE, Lee SJ, Loukidis D (2021) Numerical modelling of large deformation problems in geotechnical engineering: a state-of-the-art review. Soils Found 61(6):1718–1735. https://doi.org/10.1016/j.sandf.2021.08.007

Bathrellos GD, Skilodimou HD, Chousianitis K, Youssef AM, Pradhan B (2017) Suitability estimation for urban development using multi-hazard assessment map. Sci Total Environ 575:119–134. https://doi.org/10.1016/j.scitotenv.2016.10.025

Bathrellos GD, Skilodimou HD, Zygouri V, Koukouvelas IK (2021) Landslide: A recurrent phenomenon? Landslide hazard assessment in mountainous areas of central Greece. Z Geomorphol 63:95–114. https://doi.org/10.1127/zfg/2021/0670

Chen G, Deng W, Lin M, Lv J (2023) Slope stability analysis based on convolutional neural network and digital twin. Nat Hazards 118(2):1427–1443. https://doi.org/10.1007/s11069-023-06055-1

Chen W-F (1975) Limit analysis and soil plasticity. Elsevier, Amsterdam

Cheng C, An J, Kang J, Zeng J, Liu F (2023) A novel method for generation of random aggregate structure and its application in soil-rock mixture. Eng Anal Bound Elem 155:956–965. https://doi.org/10.1016/j.enganabound.2023.07.029

Coli N, Berry P, Boldini D, Bruno R (2012) The contribution of geostatistics to the characterisation of some bimrock properties. Eng Geol 137:53–63. https://doi.org/10.1016/j.enggeo.2012.03.015

Dyson AP, Tolooiyan A (2018) Optimisation of strength reduction finite element method codes for slope stability analysis. Innov Infrastruct Solut 3(1):38. https://doi.org/10.1007/s41062-018-0148-1

Dyson AP, Tolooiyan A (2019) Prediction and classification for finite element slope stability analysis by random field comparison. Comput Geotech 109:117–129. https://doi.org/10.1016/j.compgeo.2019.01.026

Gao W, Chen X, Wang X, Hu C (2021) Novel strength reduction numerical method to analyse the stability of a fractured rock slope from mesoscale failure. Eng Comput 37:2971–2987. https://doi.org/10.1007/s00366-020-00984-2

Griffiths DV, Lane PA (1999) Slope stability analysis by finite elements. Geotechnique 49(3):387–403

Huang XW, Yao ZS, Wang W, Zhou AZ, Jiang P (2021) Stability analysis of soil-rock slope (SRS) with an improved stochastic method and physical models. Environ Earth Sci 80:1–21. https://doi.org/10.1007/s12665-021-09939-2

Kanungo DP, Pain A, Sharma S (2013) Finite element modeling approach to assess the stability of debris and rock slopes: a case study from the Indian Himalayas. Nat Hazards 69:1–24. https://doi.org/10.1007/s11069-013-0680-4

Karpouza M, Chousianitis K, Bathrellos GD, Skilodimou HD, Kaviris G, Antonarakou A (2021) Hazard zonation mapping of earthquake-induced secondary effects using spatial multi-criteria analysis. Nat Hazards 109:637–669. https://doi.org/10.1007/s11069-021-04852-0

Khorasani E, Amini M, Hossaini MF, Medley E (2019) Statistical analysis of bimslope stability using physical and numerical models. Eng Geol 254:13–24. https://doi.org/10.1016/j.enggeo.2019.03.023

Kokusho T, Hara T, Hiraoka R (2004) Undrained shear strength of granular soils with different particle gradations. J Geotech Geoenviron 130(6):621–629. https://doi.org/10.1061/(ASCE)1090-0241(2004)130:6(621)

Li C, Chen G, Guo L, Gao J, Peng X, Yu P (2022) Slope stability and post-failure analysis of soil-rock-mixture using the modified 2D DDA-SPH method. Int J Rock Mech Min 157:105170. https://doi.org/10.1016/j.ijrmms.2022.105170

Lianheng Z, Dongliang H, Shuaihao Z, Xiao C, Yibo L, Min D (2021) A new method for constructing finite difference model of soil-rock mixture slope and its stability analysis. Int J Rock Mech Min 138:104605. https://doi.org/10.1016/j.ijrmms.2020.104605

Liu S, Wang H, Xu W, Cheng Z, Xiang Z, Xie WC (2020a) Numerical investigation of the influence of rock characteristics on the soil-rock mixture (SRM) slopes stability. KSCE J Civ Eng 24:3247–3256. https://doi.org/10.1007/s12205-020-0034-1

Liu X, Su M (2023) Double strength reduction method for slope stability analysis based on water content variation: a study and engineering application. Water 15(6):1194. https://doi.org/10.3390/w15061194

Liu S, Su Z, Li M, Shao L (2020b) Slope stability analysis using elastic finite element stress fields. Eng Geol 273:105673. https://doi.org/10.1016/j.enggeo.2020.105673

Lu Y, Tan Y, Li X (2018) Stability analyses on slopes of clay-rock mixtures using discrete element method. Eng Geol 244:116–124. https://doi.org/10.1016/j.enggeo.2018.07.021

Lu Y, Tan Y, Li X, Liu CN (2017) Methodology for simulation of irregularly shaped gravel grains and its application to DEM modeling. J Comput Civ Eng 31(5):04017023. https://doi.org/10.1061/(ASCE)CP.1943-5487.0000676

Matsui T, San KC (1992) Finite element slope stability analysis by shear strength reduction technique. Soils Found 32(1):59–70

Medley EW, Sanz Rehermann PF (2004) Characterization of bimrocks (rock/soil mixtures) with application to slope stability problems. In proceedings: EUROCK.

Meng QX, Wang HL, Xu WY, Cai M (2018) A numerical homogenization study of the elastic property of a soil-rock mixture using random mesostructure generation. Comput Geotech 98:48–57. https://doi.org/10.1016/j.compgeo.2018.01.015

Napoli ML, Barbero M, Ravera E, Scavia C (2018) A stochastic approach to slope stability analysis in bimrocks. Int J Rock Mech Min 101:41–49. https://doi.org/10.1016/j.ijrmms.2017.11.009

Napoli ML, Barbero M, Scavia C (2021) Effects of block shape and inclination on the stability of melange bimrocks. Bull Eng Geol Environ 80:7457–7466. https://doi.org/10.1007/s10064-021-02419-8

Peng S, Liao W, Liu E (2020) Pipe–soil interaction under the rainfall-induced instability of slope based on soil strength reduction method. Energy Rep 6:1865–1875. https://doi.org/10.1016/j.egyr.2020.07.012

Simoni A, Houlsby GT (2006) The direct shear strength and dilatancy of sand–gravel mixtures. Geotech Geol Eng 24:523–549. https://doi.org/10.1007/s10706-004-5832-6

Skilodimou HD, Bathrellos GD (2021) Natural and technological hazards in urban areas: assessment. Plan Solut Sustain 13(5):8301. https://doi.org/10.3390/su13158301

Sun G, Lin S, Zheng H, Tan Y, Sui T (2020) The virtual element method strength reduction technique for the stability analysis of stony soil slopes. Comput Geotech 119:103349. https://doi.org/10.1016/j.compgeo.2019.103349

Varnes DJ (1984) Landslide hazard zonation: a review of principles and practice. UNESCO, Paris, pp 1–63

Wang S, Chen G, Zhang L, Yuan J (2021a) Triaxial discrete element simulation of soil–rock mixture with different rock particle shapes under rigid and flexible loading modes. Int J Geomech 21(8):04021142. https://doi.org/10.1061/(ASCE)GM.1943-5622.0002081

Wang S, Zhu Y, Ma W, Wang Z, Li G (2021b) Effects of rock block content and confining pressure on dynamic characteristics of soil-rock mixtures. Eng Geol 280:105963. https://doi.org/10.1016/j.enggeo.2020.105963

Wang ZM, Kwan AKH, Chan HC (1999) Mesoscopic study of concrete I: generation of random aggregate structure and finite element mesh. Comput Struct 70:533–544. https://doi.org/10.1016/S0045-7949(98)00177-1

Wei HZ, Xu WJ, Xu XF, Meng QS, Wei CF (2018) Mechanical properties of strongly weathered rock–soil mixtures with different rock block contents. Int J Geomech 18(5):04018026. https://doi.org/10.1061/(ASCE)GM.1943-5622.0001131

Xiang X, Zi-Hang D (2017) Numerical implementation of a modified Mohr-Coulomb model and its application in slope stability analysis. J Mod Transport 25:40–51. https://doi.org/10.1007/s40534-017-0123-0

Xinglong Y, Jinyu D, Handong L, Shuokang B (2024) Seismic dynamic response characteristics and failure mechanisms of an accumulation body slope. Nat Hazards, pp 1–23. https://doi.org/10.1007/s11069-024-06451-1

Xu WJ, Hu LM, Gao W (2016) Random generation of the meso-structure of a soil-rock mixture and its application in the study of the mechanical behavior in a landslide dam. Int J Rock Mech Min 86:166–178. https://doi.org/10.1016/j.ijrmms.2016.04.007

Xu WJ, Yue ZQ, Hu RL (2008) Study on the mesostructure and mesomechanical characteristics of the soil–rock mixture using digital image processing based finite element method. Int J Rock Mech Min 45(5):749–762. https://doi.org/10.1016/j.ijrmms.2007.09.003

Yang Y, Chen T, Wu W, Zheng H (2021) Modelling the stability of a soil-rock-mixture slope based on the digital image technology and strength reduction numerical manifold method. Eng Anal Bound Elem 126:45–54. https://doi.org/10.1016/j.enganabound.2021.02.008

Yang Y, Sun Y, Sun G, Zheng H (2019) Sequential excavation analysis of soil-rock-mixture slopes using an improved numerical manifold method with multiple layers of mathematical cover systems. Eng Geol 261:105278. https://doi.org/10.1016/j.enggeo.2019.105373

Yang Y, Wu W, Zheng H (2023) Investigation of slope stability based on strength-reduction-based numerical manifold method and generalized plastic strain. Int J Rock Mech Min 164:105358. https://doi.org/10.1016/j.ijrmms.2023.105358

Yu J, Zhang Q, Wu C, Jia C (2023) Investigation on stability of soil–rock mixture slope with discrete element method. Environ Earth SCI 82(19):449. https://doi.org/10.1007/s12665-023-11107-7

Zhang HY, Xu WJ, Yu YZ (2016) Triaxial tests of soil–rock mixtures with different rock block distributions. Soils Found 56(1):44–56. https://doi.org/10.1016/j.sandf.2016.01.004

Zhao L, Qiao N, Huang D, Zuo S, Zhang Z (2022) Numerical investigation of the failure mechanisms of soil–rock mixture slopes by material point method. Comput Geotech 150:104898. https://doi.org/10.1016/j.compgeo.2022.104898

Zheng H, Liu DF, Li CG (2005) Slope stability analysis based on elasto-plastic finite element method. Int J Numer Meth Eng 64(14):1871–1888. https://doi.org/10.1002/nme.1406

Zhongfeng Y, Yuqin D, Jiangong C (2021) Stability analysis of rock-soil mixture slope. IOP Conf. Ser. Earth Environ Sci 638(1):012099. https://doi.org/10.1088/1755-1315/638/1/012099

Zienkiewicz OC, Humpheson C, Lewis RW (1975) Associatedand non-associatedvisco plasticity and plasticity in soil mechanics. Geotechnique 25(4):671–689